The Astrophysical Journal, 789:144 (12pp), 2014 July 10 doi:10.1088/0004-637X/789/2/144

QUASI-STATIC MODEL OF COLLIMATED JETS AND RADIO LOBES. I. ACCRETION DISK AND JETS

Stirling A. Colgate[1], T. Kenneth Fowler[2], Hui Li[1], and Jesse Pino[3]
[1] Theoretical Division, Los Alamos National Laboratory, Los Alamos, NM 87545, USA
[2] University of California, Berkeley, CA 94720, USA
[3] Lawrence Livermore National Laboratory, Livermore, CA 94550, USA
Received 2014 March 3; accepted 2014 May 25; published 2014 June 24

ABSTRACT

This is the first of a series of papers showing that when an efficient dynamo can be maintained by accretion disks around supermassive black holes in active galactic nuclei, it can lead to the formation of a powerful, magnetic helix that could explain both the observed radio jet/lobe structures on very large scales and ultimately the enormous power inferred from the observed ultra-high-energy cosmic rays. In this work, we solve a set of one-dimensional equations similar to the steady-state standard accretion disk model, but now including the large-scale magnetic fields giving rises to jets. We find that the frequently made assumption that large-scale fields are frozen into the disk is fundamentally incorrect, due to the necessity for current and the accreting mass to flow perpendicular to magnetic flux surfaces. A correct treatment greatly simplifies the calculations, yielding fields that leave the disk nearly vertically with magnetic profiles uniquely determined by disk angular momentum conservation. Representative solutions of the magnetic fields in different radial regions of the disk surface are given, and they determine the overall key features in the jet structure and its dissipation, which will be the subjects of later papers.

Key words: accretion, accretion disks – magnetic fields – magnetohydrodynamics (MHD) – galaxies: active – galaxies: jets

Online-only material: color figure

1. INTRODUCTION

Observations of powerful radio jets and lobes produced by supermassive black holes (SMBHs) at the centers of active galactic nuclei (AGNs) and the identification of radio-frequency emissions as synchrotron radiation have suggested that large-scale magnetic fields threading accretion disks play an essential role in jet formation and propagation (e.g., Lovelace 1976; Blandford 1976; Blandford & Znajek 1977; Bridle & Perley 1984; Spruit 2010; Beskin 2010). The fact that jets created by SMBHs are believed to carry a significant fraction of the SMBH energy (e.g., Burbidge 1956; Kronberg et al. 2001) has led to speculations that radio jets/lobes are the most likely candidates as accelerators producing the observed Ultra High Energy Cosmic Rays (UHECRs) up to $\approx 10^{20}$ eV. This is the first of a series of papers following up on Colgate & Li (2004), which proposed radio jet/lobes as the engine of UHECRs and suggested that plasma devices in the laboratory can help us understand jet/lobes as accelerators. This paper addresses the creation of jets by accretion disks, which will be followed by subsequent papers on jet propagation and cosmic ray generation.

Not all AGNs produce jets, and the radio-loud AGNs that do so continue to pose challenging problems: to understand how jets are launched, how they remain stable over enormous distances, how the enormous energy of jets affects the intra-cluster or inter-galactic medium through which jets pass, and how these interactions might provide feedback to the accretion disks themselves. Though not observed directly, large-scale poloidal magnetic fields threading accretion disks were suggested to play an essential role in producing the jets (e.g., Lovelace 1976; Blandford 1976; Beckwith et al. 2008). In addition, a hydromagnetic model with large-scale poloidal magnetic fields as proposed by Blandford & Payne (1982) has been widely studied and was considered to be the most promising model for launching jets and outflows from disks. This model established the significance of the angle of inclination or "tilt" of the poloidal magnetic fields lines to the plane of the disk. This angle has to be small enough ($<60^\circ$) for jet production from the surface of the disk. On the other hand, as pointed out by Lovelace (1976), magnetically dominated jets can be ejected quasi-statically along purely vertical fields by means of an electrostatic sheath, giving structures like the magnetic towers described by Lynden-Bell (e.g., Lynden-Bell 2003, 2006; Li et al. 2001, 2006).

Our goal, first explored in Fowler et al. (2011), is to use conservation laws as a way to avoid solving two-dimensional (2D) mean field equations for combined disk+jet systems in detail. In this, we extend the pioneering approaches of Shakura & Sunyaev (1973) for unmagnetized accretion disks and Solov'ev's application of fluid conservation laws to magnetized plasmas (Solov'ev 1963; Beskin 2010). In addition, using the fact that accretion disks with current flows across flux surfaces cannot obey the ideal MHD Ohm's Law, we attempt to show that given an extensive coherent polodial magnetic field supported by the disk, the conservation of disk angular momentum alone can cause this field to dominate accretion, jet ejection, and particle acceleration within the jet, even though non-magnetic processes may be important inside the disk near the black hole.

The origin of large-scale magnetic fields remains a mystery. Two main suggestions have received much discussion. One is MHD advection of ambient magnetic flux accreting toward the black hole, which assumes pre-existing coherence in a much larger environment (see discussion in Guilet & Ogilvie 2012). The other is the creation of a self-excited dynamo amplifying a seed magnetic field, in which disk rotation itself imposes coherence, either initiated from noise, as in most MHD simulations, or from finite externally driven disturbances, notably star-disk collisions (Pariev & Colgate 2007). In our model, the system has achieved quasi-steady state, either solely by advection or, more likely, by self-excitation of a seed field.

The main theoretical contribution in this paper is the use of a hyper-resistive Ohm's Law to derive accretion due to magnetic fluctuations, yielding an ordering scheme that systematically

eliminates processes competing with magnetic dominance in accretion disks. Our ordering causes jets to be launched along purely vertical field lines by means of an electrostatic sheath, which is discussed in detail in subsequent papers. Thus, our results differ from the widely studied hydromagnetic model of Blandford & Payne (1982) in which jets are launched by centrifugal forces along magnetic field lines that are sufficiently tilted with respect to the axis of rotation. With only the black hole mass and accretion rate as key inputs, we will claim model self-consistency based on both theory and derived physical quantities that are consistent with observations. Taken together, the papers in this series will try to establish a framework along with supplying details that will explain a number of observations, including jet dimensions, synchrotron radiation, and cosmic rays.

This paper is organized as follows. In Section 2, we present the main focus of this paper and the conditions to create a coherent dynamo suited to that purpose. In Sections 3 and 4, we review models coupling dynamo angular momentum to the coronal magnetic field, simplified to one-dimensional (1D) by an ordering scheme dropping B_r, justified in Section 4 and Appendix A. In Section 5, we exploit the simplicity of our 1D model to derive in detail magnetic field profiles in the disk corona extending to jets. It is these coronal/jet fields that in subsequent papers, are shown to create jets that serve as steady-state accelerators of UHECRs. In Section 6, we summarize results and compare our model with other models and simulations. In Appendix A, we discuss model closure using a hyper-resistive Ohm's law. In Appendix B, we reconcile our model with helicity conservation and Cowling's anti-dynamo theorem.

We use a stationary system of cylindrical coordinates $\{r, \phi, z\}$ in which the disk spins about a fixed z-axis with an angular frequency of $\mathbf{\Omega}$ pointing along the $+\hat{z}$ direction. The jet current j_z is taken along the $+\hat{z}$ direction in the inner region of the disk, giving positive B_ϕ and negative B_z in the same region. Units are in cgs, often introducing c, the speed of light.

2. THE FOCUS OF THIS PAPER

We represent the disk–jet system schematically in Figure 1, showing that as the dynamo develops in a disk (at the bottom of the figure), the disk ejects a strong current in the Central Column inside a radius $r \leqslant a$ that is the nearest to the black hole, with decreasing current density in a Diffuse Pinch region that is surrounding the Central Column. The current ejected from the accretion disk will return at a Nose region, coming back to the disk along an outer boundary that is presumably bounded by the surrounding plasma pressure in the inter-stellar medium, intra-cluster medium, or the inter-galactic medium, depending on the extent and environment the jets pass through. However, these details are not important for our model.

2.1. Jets Ejected by an Accretion Disk Dynamo

The main purpose of this paper is to derive the coronal magnetic field at the disk surface, to be used as a boundary condition in calculating magnetic (Poynting) jet propagation in subsequent papers. The resulting jet is represented in Figure 1 by an overlay of magnetic flux surfaces actually calculated using the well-known Grad–Shafranov method (Beskin 2010).

We first note that a dynamo would always try to create jets. We use the term dynamo to describe a rotating accretion disk permeated by a poloidal magnetic field (B_z). If a poloidal field of

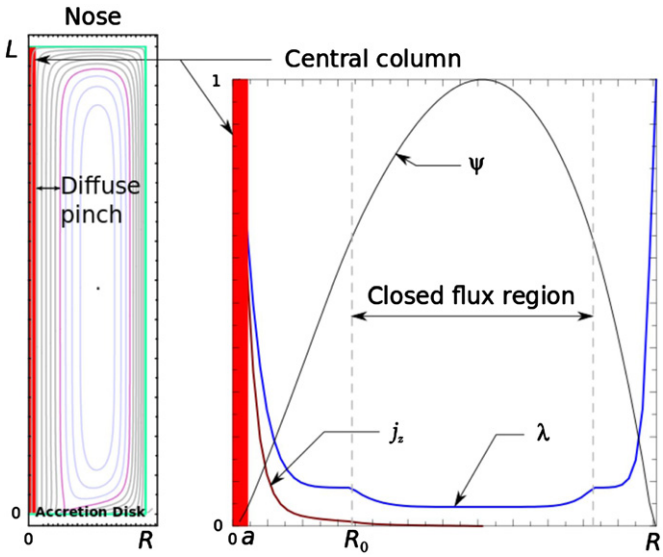

Figure 1. Left: a simplified sketch of an accretion disk ejecting a jet, overlaid by a Grad–Shafranov solution for the cross-section of poloidal (B_z, B_r) magnetic flux surfaces, for the accretion disk boundary condition derived in Section 5.1 depicted in Figure 2. The axisymmetric calculation box is a cylinder of radius R and height L. The jet current is concentrated in a Central Column of radius a calculated in the text, surrounded by a Diffuse Pinch of radius R_0 and an extended outer region of radius R bounded by the return current. Note that outgoing flux surfaces are straight, finally turning at the "nose" (right). Also drawn are the poloidal flux function Ψ, the poloidal current j_z, and the function $\lambda = |j_z/B_z|$ depicted at $z = L/2$ midway up the column.

(A color version of this figure is available in the online journal.)

a fixed sign extends over a radial dimension d, the mere presence of this field guarantees that differential rotation will charge up the disk over the dimension d, producing an anode at the edge nearest to the black hole for our sign convention.

In Appendix B, we will argue that any patch of field advected to the vicinity of the black hole will feed off the gravitational power concentrated near the black hole. The first patch to do so will soon dominate so that this field patch growing to a large radius becomes the source of the visible jet. Charging of this patch of field produces an EMF that drives the jet current between inner and outer footprints of poloidal field lines exiting and returning to the disk, the inner footprint acting as an "anode" (Lovelace 1976). As we will see in the subsequent papers in this series, the accelerator physics is simplest when ions are ejected at the inner footprint serving as an anode, hence our sign convention $j_z > 0$. With this convention, as sketched in Figure 1, the returning current loops are closed inside the disk by a current density j_r pointing toward the black hole, flowing perpendicular to magnetic flux surfaces inside the disk. The j_r direction inside the disk is also opposite to a positive $E_r = -c^{-1} r \Omega B_z$ with $B_z < 0$ for $\Omega > 0$ and $B_\phi > 0$ whereby the term $j_r E_r < 0$ extracts power from the disk rotation. When strong enough, these current loops stretch vertically to create highly elongated jets.

2.2. Origin of the Coherent Dynamo Magnetic Field

As noted in the Introduction, the origin of the large-scale coherent magnetic fields essential for astrophysical jets remains a mystery. In the main text, we will simply assume the existence of a large-scale B_z and defer further comments on the origin of B_z to Appendix B. As a related topic, we also show in Appendix B that our model is consistent with the conservation of helicity. Our main contribution is to show that however a

coherent poloidal field is produced, the properties of jets can be derived using the heuristic properties of the accretion disk and that this can be done mostly independent of other details of disk dynamics (see Sections 3–5).

That explaining the origin of the coherent poloidal fields is the key remaining issue has been elucidated by recent experiments. A self-excited dynamo requires coupled amplification of the toroidal field when using a given poloidal field and vice versa. Given a poloidal field, experiments have now demonstrated for the first time an eight-fold amplification of the toroidal field in a liquid metal plasma surrogate (Colgate et al. 2011).

3. THEORY OF QUASI-STATIC DISK/JET SYSTEMS

Next, we consider briefly the theory of accretion disks, keeping only what is needed to calculate the coronal magnetic fields, the main objective of this paper. The pioneering work on accretion disks, summarized in Frank et al. (2002), is that of Shakura & Sunyaev (1973), not yet taking into account the role of global magnetic fields that are threading the disk. The pioneering work by Blandford & Payne (1982) identified jet creation with the centrifugal ejection of mass along magnetic field lines tilted relative to the axis of disk rotation. All work along these lines is aimed at solving 2D equations for "mean fields" ρ (mass density), $\mathbf{v}$ (fluid velocity), and $\mathbf{B}$ (magnetic field), where we define "mean field" as an axisymmetric average over fluctuations in time and space (see review in Beskin 2010). Except very near the black hole, the equations needing to be solved are Faraday's Law coupled to the following non-relativistic equations for mass and momentum conservation:

$$\partial\rho/\partial t + \nabla\cdot(\rho\mathbf{v}) = 0 \tag{1}$$

$$\rho[\partial\mathbf{v}/\partial t + \mathbf{v}\cdot\nabla\mathbf{v}] = (1/4\pi)(\nabla\times\mathbf{B})\times\mathbf{B} - \rho\nabla\Phi_G - \nabla p - \nabla\cdot\underline{\mathbf{T}}, \tag{2}$$

where we use $\mathbf{j} = (c/4\pi)\nabla\times\mathbf{B}$ and p is plasma pressure. The viscous stress tensor $\underline{\mathbf{T}} = -\rho\nu[\nabla\mathbf{v} + (\nabla\mathbf{v})^{\mathrm{T}} - (2/3)(\nabla\cdot\mathbf{v})\mathbf{I}]$ contains the kinematic viscosity ν used in the Shakura-Sunyaev standard model, giving an accretion velocity $v_r = -(3/2)(\nu/r)$ for Keplerian rotation (Krolik 1999; Frank et al. 2002). In our model, ν will also include the Maxwell stress due to magnetic fluctuations (see Appendix A.2). In Equation (2), we have dropped $\mathbf{E}(\nabla\cdot\mathbf{E}/4\pi)$ where $\mathbf{E}$ is the electric field, since this term is small to order $(r\Omega/c)^2$ compared to magnetic terms. We defer applying Faraday's Law to Section 4 and Appendix A.

3.1. Steady Accretion Rate

Except near the radius $r = R_0$, where $B_z = 0$ (the O point, see Figure 1), quantities evolve at a rate equal to the rate of the power that arrives to produce this growth, namely, at the mass accretion rate $\dot{M} = dM/dt$ with black hole mass M. We take both M and $\dot{M}$ to be input parameters, where at any radius r, we have (Frank et al. 2002)

$$\dot{M} = \int_{-H}^{H} dz 2\pi r|v_r|\rho \approx 4\pi r|v_r|\rho H, \tag{3}$$

where both v_r and ρ are representative values inside the disk. This follows from Equation (1) if we drop $\partial\rho/\partial t$, integrate vertically with half-height H and set $v_z = 0$ at $z = 0$, H, justified later, showing that $\int_0^H dz\partial(rv_r\rho)/\partial r \approx \partial(\int_0^H dz r v_r\rho)/\partial r = 0$. For this boundary condition, $\dot{M}$ is a constant in a steady disk and is independent of r.

3.2. Quasi-static Momentum Equations

To calculate the coronal magnetic field, which is our main objective, again we assume a quasi-steady state, and $\mathbf{B} = \{B_r, B_z, B_\phi\}$ are axisymmetric mean field quantities smooth-averaged over fluctuations in time and space. We keep only the $r-$component and angular momentum component obtained by operating $\mathbf{z}\cdot(\mathbf{r}\times)$ on Equation (2), giving

$$\left\{\rho\mathbf{v}\cdot\nabla v_r + (\nabla\cdot\underline{\mathbf{T}})_r - \frac{B_z}{4\pi}\frac{\partial B_r}{\partial z}\right\} = -\frac{1}{8\pi}\left[\frac{\partial B_z^2}{\partial r} + \frac{1}{r^2}\frac{\partial\left(r^2B_\phi^2\right)}{\partial r}\right] - \left[r\rho\left(\Omega_K^2 - \Omega^2\right) + \frac{\partial p}{\partial r}\right] \tag{4}$$

$$\left\{\frac{(\partial\rho v_z r^2\Omega)}{\partial z} + r\frac{\partial T_{z\phi}}{\partial z}\right\} + \frac{1}{r}\frac{\partial(r\rho v_r r^2\Omega[1-(\nu/v_r)\partial(\ln\Omega)/\partial r])}{\partial r} = \frac{r}{c}(j_z B_r - j_r B_z) = \frac{1}{4\pi}\frac{\partial(rB_\phi B_z)}{\partial z} + \left\{\frac{1}{4\pi r}\frac{\partial(r^2B_r B_\phi)}{\partial r}\right\}. \tag{5}$$

Here $\Omega_K^2 = GM/r^3$ is the Keplerian rotation with Newtonian gravitational constant G, and p is the plasma pressure. On the left-hand side (LHS) of Equation (5), we approximate $T_{r\phi}$ by a scalar viscosity ν representing transport both by velocity and magnetic fluctuations (see Balbus & Hawley 1998, Equation (35)). On the right-hand side (RHS) of Equation (5), we add and subtract $rB_\phi(\partial B_z/\partial z) = -B_\phi\partial(rB_r)/\partial r$ using $\nabla\cdot\mathbf{B} = 0$. We will solve Equation (2) using an ordering scheme that will be justified later. In order to compare our work with that of others, these equations are written in a form displaying in {...} the terms that we will drop, which we argue will allow us to focus on the magnetically dominated limit with strong magnetic jets ejected from the accretion disk surface.

4. A SIMPLIFIED MODEL OF DYNAMO/JET COUPLING

We will now review 1D models of accretion disks constructed by adding the magnetic field to the 1D standard model of Shakura and Sunyaev (Frank et al. 2002). In this section, we are mainly concerned with the extended Diffuse Pinch zone at $r > a$ (see Figure 1). Because all jet currents returning to the disk must flow downward through the Diffuse Pinch zone, understanding this zone will help us understand the current and power in the Central Column zone of Figure 1 where most of the gravitational power is deposited. The Central Column, containing most of the jet current, will turn out to be highly concentrated with a radius perhaps 10 times that of the black hole (see discussions in Section 5).

4.1. A Simplified Set of Equations

Before we discuss the mathematical treatment of Equations (4) and (5), we can make some general observations: the hydrodynamic terms describe the mass and angular momentum transport within the disk, while the magnetic terms describe magnetic transport of that portion coupled to the field. The quantity $\partial(rB_\phi B_z/4\pi)/\partial z$ in Equation (5) concerns the vertical launch of a jet in the Diffuse Pinch zone. The terms associated with B_r correspond to the possible vertical outflow of plasma from the disk. Whereas all hydrodynamic terms are proportional to the density ρ which dominates inside the disk, the magnetic terms can extend beyond the disk scale height and

become dominant. It is this common linkage of the disk and jet/lobe accelerator by the magnetic field that simplifies our model, the main effect of the field on the disk being contained in the accretion velocity v_r that we have absorbed in $\dot{M}$ as an input parameter in Equation (3).

Unlike the studies by Lovelace et al. (2009) and Guilet & Ogilvie (2012, 2013), we do not attempt to obtain details inside the disk. Instead, consistent with our objectives, we seek only magnetic field solutions at the disk surface at $z = H$ (the corona) where the jet joins the disk. As noted in Bisnovatyi-Kogan & Lovelace (2012), the fact that the jet begins where the gravity-induced accretion ceases suggests a set of boundary conditions at this coronal surface, namely, ρ, v_r, v_z and $p \to 0$ as $z \to H$. (It is this boundary condition on v_z that yields constant $\dot{M}$ in Equation (3).) Furthermore, anticipating that magnetic hoop forces mentioned in Section 4.2 will straighten flux surfaces in the jet, we make an additional simplifying assumption on the boundary condition that $B_r \approx 0$ at $z = H$.

Applying these boundary conditions to Equation (4), we see that all the hydrodynamic terms as well as the term involving B_r can be dropped, giving in the corona

$$\frac{\partial B_z^2}{\partial r} + \frac{1}{r^2}\frac{\partial\left(r^2 B_\phi^2\right)}{\partial r} = 0; \text{ at } z = H. \tag{6}$$

On closer inspection, this equation could have been written out of hand as that appropriate to any pressureless cylindrical magnetic field configuration self-confined by pinch forces, the likely description of jets maintaining collimation far beyond disk dimensions.

Equation (5) provides a constraint relating B_z and B_ϕ. To see this, we multiply Equation (5) by 4π and integrate it over $0 < z < H$. Assuming for a moment that we can drop all the terms in {...}, we get

$$g[(\dot{M}/2)\Omega_K] = (r B_\phi |B_z|)_{r,H}; \tag{7}$$

$$g = [(\dot{M}/2)\Omega_K]^{-1}\int_0^H dz(4\pi/r)\partial/\partial r \times \{r\rho|v_r|r^2\Omega[1 + (\nu/|v_r|)\partial(\ln\Omega)/\partial r]\}, \tag{8}$$

where g is dimensionless and it signifies the fraction of the angular momentum extracted by the jet, normalized by a factor Ω_K giving $g = 1$ for zero viscosity and Keplerian rotation (see Appendix A.2). Note that while disks can eject jets up and down, hereafter we will discuss only the upward jet in Figure 1, thus requiring the factor 1/2 in Equations (7) and (8) since only half of $\dot{M}$ feeds the upward jet. We have implicitly assumed that $v_r < 0$; and B_z is negative at the inner disk according to our sign convention. In Equation (7), we have used $B_\phi = 0$ at $z = 0$, giving on the RHS only the coronal field components at radius r and $z = H$. Equation (7) with magnetic terms in this form appears also in Lovelace et al. (2009), after their Equation (8) but with different notation and a specific $\nu = \alpha H c_S$ of the standard model form.

Dropping terms in {...} in Equation (5) is justified as follows. As noted in Lovelace et al. (2009), boundary conditions give zero upon integrating the dropped hydrodynamic terms. To drop the magnetic term in {...} on the RHS, we only need to require that this term be small compared to the magnetic term retained. Assuming that $\partial/\partial z \sim 1/H$ and $\partial/\partial r \sim 1/r$, the ratio of the magnetic term in {...} to the term retained is, approximately,

$$\delta r/r \equiv (B_r/B_z)(H/r) \approx |v_r/v_K| \ll 1, \tag{9}$$

where $\delta r/r$ is a measure of field line tilt inside a disk of scale height H, and the accretion velocity v_r and Keplerian rotation $v_K = r\Omega_K$ are representative values inside the disk.

Here, we introduce $|v_r/v_K| \ll 1$ as the smallness parameter for our disk model, in contrast with Mach numbers v/v_A characterizing fluid effects in magnetic jets (e.g., Beskin 2010). While all quantities vary with r, and it is generally thought that $|v_r/v_K|$ should be taken small (e.g., Lovelace et al. 2009), the special significance of $|v_r/v_K|$ being small at all r inside disks is suggested by the following mean-field hyper-resistive Ohm's Law yielding Faraday's Law:

$$\begin{aligned}\mathbf{E} + c^{-1}\mathbf{v}\times\mathbf{B} &= -c^{-1}\partial\mathbf{A}/\partial t - \nabla\Phi + c^{-1}\mathbf{v}\times\mathbf{B}\\ &= -c^{-1}\langle\mathbf{v_1}\times\mathbf{B_1}\rangle \equiv \mathcal{D}.\end{aligned} \tag{10}$$

Here, the fields $\mathbf{E}$, $\mathbf{A}$, Φ, $\mathbf{v}$, and $\mathbf{B}$ are 2D mean fields averaged over ϕ and averaged over symmetric fluctuations in space and time so as to give smooth quantities with no evidence of ripples due to the fluctuations. Here $\mathbf{A}$ is the vector potential whereby the poloidal flux function rA_ϕ gives rise to the poloidal field B_z. The Spitzer resistivity, small for the accretion disk, is replaced by hyper-resistivity $\mathcal{D}$ due to magnetic fluctuations and turbulence (Boozer 1986a; Fowler & Gatto 2007). Except near the O point discussed in Appendix B, in quasi-steady state, we can drop $\partial\mathbf{A}/\partial t \approx \mathbf{A}/\tau$, giving

$$(-c\partial\Phi/\partial r + v_\phi B_z) - v_z B_\phi \approx -v_z B_\phi = c\mathcal{D}_r, \tag{11a}$$

$$v_z B_r - v_r B_z \approx -v_r B_z = c\mathcal{D}_\phi, \tag{11b}$$

$$v_r B_\phi - v_\phi B_r = c\mathcal{D}_z. \tag{11c}$$

Components of $\mathbf{B}$ and $\mathbf{v}$ are those inside the disk, where v_ϕ and the dynamo electrostatic field $-\partial\Phi/\partial r$ are dominant so that $(-c\partial\Phi/\partial r + v_\phi B_z) \approx 0$ in Equation (11a). Also, the boundary condition $v_z = 0$ at $z = 0, H$ introduced in Section 4 implies that for an accretion flow to fit inside the $z = H$ boundary, we require, on average,

$$v_z \approx (z/r)v_r \leqslant (H/r)v_r. \tag{12}$$

The simplification in Equation (11b) is obtained by noting that $|v_z B_r/v_r B_z| \approx |(B_r/B_z)(H/r)| = \delta r/r \ll 1$ using Equations (12) and (9). Then Equation (11b) allows us to relate the toroidal component of hyper-resistivity to the diffusion coefficient D_a giving the accretion velocity v_r that appears in our ordering parameter $|v_r/v_K|$, giving

$$v_r \approx -(c\mathcal{D}_\phi/B_z) \equiv -(D_a/r), \tag{13}$$

where we have used the standard formulation relating diffusion D_a and accretion velocity.

Taking the ratio of Equations (11a) and (11b), and using Equation (12), we get an expression for H; while Equation (11c) gives an expression for B_r inside the disk:

$$\begin{aligned}\zeta &\equiv |HB_\phi/rB_z| \approx |\mathcal{D}_r/\mathcal{D}_\phi|;\\ |B_r/B_\phi| &\approx |(v_r/v_\phi) - (c\mathcal{D}_z/v_\phi B_\phi)|.\end{aligned} \tag{14}$$

These equations relate the hyper-resistivity to disk quantities H and v_r.

Equation (9) follows from Equation (14) because $|\mathcal{D}_r/\mathcal{D}_\phi|$ turns out to be order unity, while $|c\mathcal{D}_z/(v_\phi B_\phi)|$ is at most of

the order of $|v_r/v_K|$, giving $|B_r/B_\phi| \approx |v_r/v_K|$. Then $\delta r/r = \zeta|v_r/v_K| \approx |v_r/v_K|$. To maintain narrative flow of the whole paper, we defer the somewhat involved heuristic derivation of these statements to Appendix A. Here and hereafter, we simply assert Equation (9) as our ordering scheme and pursue its consequences in simplifying our accretion disk model.

Our ordering can be compared with the systematic 2D ordering scheme of Guilet & Ogilvie (2012) for the early stages of accretion, before a jet is fully established (giving B_ϕ of higher order than B_z). Our 1D steady-state ordering gives their zeroth order for ρ, Ω, Ω_K but also H is zeroth order (but varying with r). Defining $\epsilon = \sqrt{|v_r/v_K|}$, we must order both B_z and B_ϕ as first order in ϵ; v_z, v_r, and p as second order; and B_r as third order. Then all quantities discarded are smaller than those retained by a factor of ϵ or ϵ^2.

4.2. Conditions for Strong Jets and Physical Interpretations

We note that Equations (6) and (7) are the most important equations for our model. The remaining uncertainty is contained in the parameter g, which represents the expulsion of angular momentum by a jet in ratio to transport by accretion. Thus we expect $0 < g \leqslant 1$, with $g = 0$ representing total transport via disk viscosity, whereas $g = 1$ represents total transport via large-scale magnetic fields into the jet. For a given accretion rate $\dot{M}$, Equations (7) and (8) say that the jet is strongest if $g = 1$, which further implies that $\Omega \approx \Omega_K$ and $\nu \approx 0$. Physically, the condition $\Omega \approx \Omega_K$ implies that the jet is driven by maximum rotation. The condition $\nu \approx 0$ implies that magnetic fields are the main agent for recycling disk angular momentum to the accretion source. In addition, the condition $B_r \approx 0$ in the Diffusion Pinch region, both in the corona and inside the disk (by Equation (9)), implies that in the Diffuse Pinch region no accretion energy is lost by centrifugal ejection as proposed by Blandford & Payne (1982).

In our model, Equation (7) provides the only linkage between the coronal magnetic fields and the disk interior where the dynamo action occurs. Equation (7) is analogous to a Faraday disk, similar to the Barlow wheel analogy in Ferreira (2003). If we replace the LHS by the drive shaft of a Faraday disk, this equation also describes jets like Figure 1, now created by a rotating metallic disk in contact with a plasma (Fowler 2004). Disk rotation excites currents exiting the Faraday disk along an applied dipole poloidal magnetic field passing through the disk. Current closure is provided by disk conductivity allowing j_r to flow across flux surfaces inside the metallic disk, giving $\partial B_\phi/\partial z = -(4\pi/c)J_r$ with $J_r < 0$, so that B_ϕ increases through the disk to a maximum value at the disk surface. Jets arise in the fringe field outside the dynamo, corresponding to the accretion disk coronal field where the disk joins the jet it creates. Initially, in this fringe field B_ϕ decreases giving an outward hoop force $(\mathbf{j} \times \mathbf{B})_z \propto -\partial B_\phi^2/\partial z > 0$, which first launches the jet and then gives $\partial B_\phi/\partial z \to 0$ and $B_r \to 0$ as the jet lengthens, as assumed in deriving Equation (6). In Appendix B, we discuss other underlying field geometries giving rise to dynamos, such as quadrupoles (Pariev & Colgate 2007; Beckwith et al. 2008), which can be regarded as having two Faraday disks back to back.

An accretion disk would become a Faraday disk early in the accretion process. Suppose that initially, ions are stuck to the field lines of a seed poloidal field B_z so that ions and flux accrete together. Collisional conductivity being negligible, initially flux surfaces act as insulation so that, even though the disk charges up like a Faraday disk, no poloidal current can flow to create a jet. Creation of a jet is due to radial transport of current and mass driven by growing magnetic fluctuations in 3D, yielding the hyper-resistive Ohm's Law in Equation (10). As fluctuations grow, the accreting ions and electrons begin to slip across flux surfaces yielding a radial current that allows a jet to be created. Jet current saturates when the jet ejects all excess angular momentum arriving at a given flux surface, giving a quasi-steady state on a timescale $t \approx r/v_r$.

Fluctuations may grow up from instabilities in disks, such as the flow-driven magnetorotational instability (MRI; e.g., Balbus & Hawley 1998), or the pressure-driven interchange (Spruit et al. 1995), or possibly the current-driven instabilities (Ebrahimi & Prager 2011). Fluctuations may also be stimulated externally, as in the star-disk collision mechanism of Pariev & Colgate (2007). Some simulations exhibit at least transient accretion by MRI (Beckwith et al. 2008), while strong evidence for current transport is shown in that coming from current-driven kink modes in spheromak experiments (Hooper 2012).

Consistent with our objectives, we will avoid needing to know details about the underlying 3D fluctuations by subsuming our ordering parameter $|v_r/v_K|$ in $\dot{M}$, both M and $\dot{M}$ being treated as input parameters as noted in Section 3. In doing so, we will not be able to derive with much certainty under what circumstances the competing physics in the parameter $g(r)$ gives a strong or weak magnetic dynamo. Thus, we choose to retain g as an undetermined parameter. All of our results can then be stated in terms of M, $\dot{M}$, and g without knowing g in advance. In Appendix A, we discuss physical assumptions giving $g \approx 1$, and hence a strong jet.

5. DETERMINING MAGNETIC FIELD STRUCTURES AT THE DISK SURFACE

This section uses the results from Section 4 to provide the information needed to calculate jet propagation and cosmic ray acceleration in subsequent papers. We begin with a physical description. The fact that gravitational power is concentrated near the black hole should cause the dynamo current driven by this power to be concentrated there also, leading us to divide the outgoing current and flux in Figure 1 into two regions, the Central Column zone ejecting most of the jet current, and a Diffuse Pinch zone with lower current density surrounding this Central Column.

A radial division of the ejected current profile is suggested also by the fact that Equation (7) coupling the dynamo to the jet is most tractable when the rotation velocity $\Omega(r)$ is a known quantity, as in the simplified version on the LHS of Equation (7), which gives Keplerian rotation when $g \approx 1$. However, Keplerian rotation cannot persist near the black hole where $r\Omega_K \to c$, and other physics becomes important in determining the radial force balance. This suggests that the Diffuse Pinch zone boundary at $r = a$ be defined as the boundary where Keplerian rotation begins to fail. Finally, in Paper II, we will find that the magnetic profiles dictated by Keplerian rotation, when projected into a jet, yield a magnetic helix/jet in which its Diffuse Pinch zone is stable to current driven instabilities, while the Central Column zone may undergo magnetic relaxation (Taylor 1986).

Separating the disk into a Keplerian Diffuse Pinch zone surrounding a Central Column zone helps to conceptualize the above physical processes in each zone. We now discuss them in more detail.

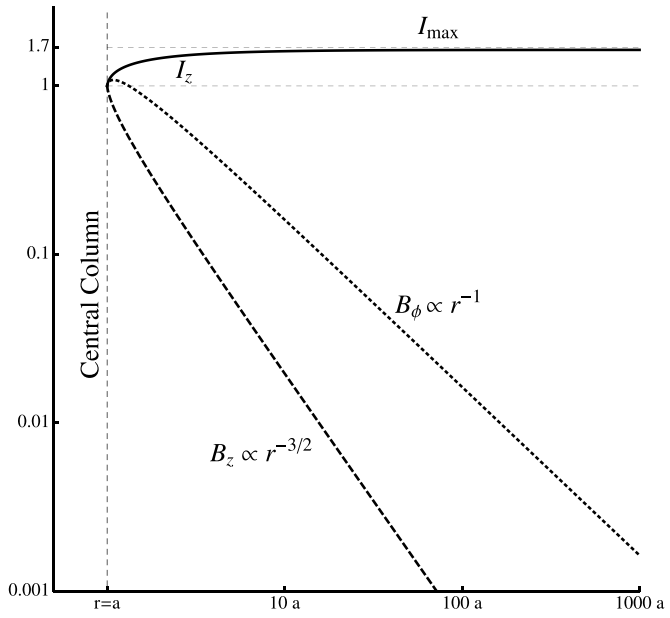

Figure 2. Distribution of the coronal magnetic field $\{B_z, B_\phi\}$ at the surface of an accretion disk in the Diffuse Pinch zone, showing the asymptotic limits $B_\phi \propto 1/r$ and $B_z \propto 1/r^{3/2}$ characteristic of a disk ejecting a Poynting-dominated jet with zero viscosity and Keplerian rotation (i.e., $g \approx 1$), as derived from the conservation of angular momentum. For finite viscosity, B_ϕ is about the same, but B_z falls faster. Matched to a magnetically relaxed Central Column region, the fields shown here serve as the boundary condition for the Grad–Shafranov solution in Figure 1. Note that B_z is plotted as positive but a negative sign should be included, given our sign convention.

5.1. Diffuse Pinch Zone, Coronal Fields

Let us first accept our ansatz that $B_r = 0$ in the corona and calculate the coronal field using Equations (6) and (7). We obtain

$$\frac{\partial B_z^2}{\partial r}+\frac{1}{r^2}\frac{\partial\left(r^2 B_\phi^2\right)}{\partial r} = \frac{\partial B_z^2}{\partial r}+\frac{1}{r^2}\frac{\partial[g(\dot{M}/2)\Omega_K/B_z]^2}{\partial r} = 0, \quad (15)$$

where we have used the definition of g in Equation (7).

To obtain a solution to Equation (15), we can explore the limiting cases either if the viscosity $\nu \approx 0$ and $\Omega \approx \Omega_K$, giving $g\dot{M}\Omega_K \propto r^{-3/2}$, or if $g\dot{M}\Omega_K$ can be written approximately as a power law in r, e.g., $g\dot{M}\Omega_K \propto r^{-K}$ with $K \geqslant 3/2$. Equation (15) can then be solved analytically by combining variables to form a dimensionless quantity, $Q = B_z^2/B_\phi^2 = B_z^4 r^2/[g(\dot{M}/2)\Omega_K]^2$, whereby Equation (15) and its solution become (Fowler et al. 2011)

$$dQ/dr = (2/r)[Q/(Q-1)][Q(K+1)+(K-1)] \quad (16)$$

$$r/R_1 = Q^{-\kappa}[(K+1)Q+(K-1)]^q, \quad (17)$$

with $\kappa = 1/(2(K-1))$ and $q = K/(K^2-1)$ and an arbitrary length-scale R_1. That Equation (17) is the solution can be verified by taking dr/dQ, inverting, and choosing κ and q to agree with Equation (16).

It turns out that the solution to Equation (17) has two branches, the appropriate one for an isolated accretion disk with fields falling off at infinity being that plotted in Figure 2 for the case of $\nu = 0$ and $\Omega = \Omega_K$ giving $K = 3/2$, $\kappa = 1$, and $q = 6/5$. There is no solution for $r/R_1 < (2K)^q \approx 3.7$, occurring at $Q = 1$ where $dr/dQ = 0$. Following up on our discussion above of what defines the boundary between the Diffuse Pinch and the Central Column, we interpret $r = a = 3.7R_1$ as the inner boundary of the Diffuse Pinch region below which Keplerian scaling is no longer possible. Solutions for finite ν giving $K > 3/2$ behave similarly, which gives the Diffuse Pinch boundary $a = (2K)^q R_1$ at $Q = 1$. Again, $Q(r)$ defined by Equation (17) gives $B_z = [Q(r)((\dot{M}/2)\Omega_K(r)g(r))^2/r^2]^{1/4}$ and from this B_ϕ by Equation (7).

A useful approximation to Figure 2 that is valid for any viscosity can be obtained if we first neglect j_z in the Diffuse Pinch portion of the coronal field giving $B_\phi(r) \approx 2I/(cr) \propto 1/r$, where I represents the total current inside the Central Column. Then using Equation (7), we have $|B_z(r)| \propto g\Omega_K(r) \propto g/r^{3/2}$. We also use the fact that $Q = 1$ defines the Diffuse Pinch boundary for any ν (any K), giving $Q = B_z^2/B_\phi^2 = 1$ at $r = a$, hence $B_\phi(a) = |B_z(a)| \equiv B_a$. Then, we get

$$B_\phi(r) \approx B_a(a/r);\ |B_z(r)| \approx B_a(a/r)^{3/2}(g/g(a)) \text{ for } r \geqslant a. \quad (18)$$

We can refine the solution $B_\phi(r)$ in Equation (18) by substituting the approximate $|B_z(r)|$ in Equation (18) into Equation (15) giving $\partial(rB_\phi)^2/\partial r = (C_1/a)(a/r)^{2K-1}$ where C_1 is left adjustable to fit the quantities shown in Figure 2. Integrating this equation introduces another adjustable integration constant which gives

$$rB_\phi(r) = C_2 a B_a[1 - C_1(a/r)^{2K-2}]^{1/2}, \quad (19)$$

where as noted both C_1 and C_2 are adjustable constants.

For Figure 2 corresponding to $g = 1$ and $K = 3/2$ (zero viscosity and Keplerian rotation), we get $C_2 = 1.7$ to fit the asymptotic limit of $I(r)$, giving $C_1 = 0.6$ to yield the Central Column current I at $r = a$ and $B_\phi = B_a$. Equation (19) gives the corrections for finite j_z in the Diffuse Pinch needed for stability analysis in subsequent papers. As shown in the figure, the Diffuse Pinch fields quickly asymptote to those in Equation (18).

The fact that $I(r)$ asymptotes to $I(r) = 1.7I$ verifies that, for $g = 1$, the total current I in the Central Column represents $1/1.7 \sim 60\%$ of the total dynamo current emanating from the disk (inside the radius R_0). That the relatively low power Diffuse Pinch dictates the current flow through the Central Column where most of the gravitational power is deposited is a defining feature of our model.

5.2. Central Column Zone: 0D Model

Concerning the Central Column, let us first suppose that the field is magnetically force free but unstable as Keplerian rotation begins to fail. If the field is then relaxed as mentioned above, we can get some idea of its profiles by continuing the solution of Equation (15), rewritten in the following form:

$$\nabla \times \mathbf{B} = \lambda(r)\mathbf{B}, \quad (20)$$

where constant λ represents magnetic relaxation (Taylor 1986). Here $\lambda = (4\pi/c)(I/\Psi(a))$ derived from $I = \int_0^a 2\pi r dr j_z$ with $4\pi j_z/c = \lambda B_z$ and total poloidal flux $\Psi(a)$ in the Central Column. Since I in the Central Column is known from the Diffuse Pinch solution, this procedure reduces the Central Column problem to an assumption of magnetic relaxation (constant λ) and a 0D model with one undetermined parameter, the Central Column flux $\Psi(a)$. However, since there is no obvious way to guess or derive $\Psi(a)$, and since the pressureless jet solution is likely to be incorrect at very small radii in any

case, we choose instead to couch the problem in terms of jet power, as follows.

We write the Central Column current I and the voltage V driving this current as

$$V = \int_0^a dr(-c^{-1}r\Omega B_z) = b[(a\Omega_a/c)aB_a], \quad (21)$$

$$I \equiv I_z = \int_0^a dr 2\pi r[(c/4\pi)r^{-1}\partial(rB_\phi)/\partial r] = aB_a c/2, \quad (22)$$

$$IV = (b/2)\left[a\Omega_a a^2 B_a^2\right] = f(\dot{M}c^2/4). \quad (23)$$

Here $b = \langle r\Omega|B_z|\rangle/(a\Omega_a B_a)$ averaged over the Central Column, and f is the efficiency for converting gravitational power into Poynting power.

5.3. An Illustrative Example

We take $b = 5$, noting that $r\Omega/(a\Omega_a) < c/(a\Omega_a) = (2a/R_s)^{1/2} \approx 5$ and $1 < |B_z|/B_a < 2$ in the Central Column, giving b as the average of a quantity ranging 1–10. Here we have taken as an illustrative B_z in the corona the solution of Equation (20) with constant λ. Expanding in powers of $x = \lambda r/2$ gives $|B_z| = B_0(1 - x^2)$ and $B_\phi = B_0 x(1 - 0.5x^2)$ giving $x \approx 2/3$ for boundary condition $B_\phi(a) = |B_z(a)| = B_a$ and $B_0/B_a = 9/5 \approx 2$. In addition, we estimate the efficiency f by first calculating the efficiency for each flux surface in the Diffuse Pinch zone. From Equation (7), the Poynting power for a single jet is $-r\Omega B_z B_\phi/(4\pi) = \dot{M}\Omega_K^2 g/(8\pi)$, which is a factor of $g/2$ smaller than half of the gravitational power driving this jet and is given by $1/2\int_{-H}^{H} dz\rho v_r(-GM/r^2) = \dot{M}\Omega_K^2/(4\pi)$. Anticipating other losses near the black hole, for f in the Central Column, we divide by another factor of 2, giving the following as our estimates:

$$b = 5;\ f = g_a/4, \quad (24)$$

where g_a is g at $r = a$.

We now solve both Equations (23) and (7) for aB_a at $r = a$ and equate the results to obtain

$$aB_a = [(f/b)(\dot{M}/2)c/(a\Omega_a/c)]^{1/2} = [(\dot{M}/2)c(a\Omega_a/c)g_a]^{1/2}. \quad (25)$$

Equating the two expressions on the RHS in Equation (25) gives the results that match the Diffuse Pinch to the Central Column. Using b and f in Equation (24), we obtain

$$a\Omega_a/c = (R_s/2a)^{1/2} = (1/4b)^{1/2} \approx 0.2, \quad (26)$$

$$a = (2b)R_s = 10R_s = 3 \times 10^{14} M_8\,\mathrm{cm}, \quad (27)$$

where $R_s = 2GM/c^2$ and $M_8 = M/(10^8 M_\odot)$. Substituting Equations (25) and (26) into Equation (21) gives the disk voltage:

$$V = b(a\Omega_a/c)aB_a = b(a\Omega_a/c)^{3/2}(g_a(\dot{M}/2)c)^{1/2}$$
$$\approx g_a^{1/2} 5 \times 10^{17} M_8^{1/2} \approx g_a^{1/2} 1.5 \times 10^{20} M_8^{1/2}\,\mathrm{volts}, \quad (28)$$

where we take $\dot{M} = M/\tau$ for a typical system lifetime $\tau = 10^8$ yrs $= 3 \times 10^{15}$ s (Colgate & Li 2004; Beskin 2010). Thus, the jet accelerator voltage V is large at $g_a = 1$ but diminishes as $g_a \to 0$.

The radius a in Equation (27) as a boundary between zones is only approximate. The 0D solution itself is valid until finally non-magnetic forces dominate very near the black hole. The dynamo region nearest the black hole was considered in the pioneering paper of Blandford & Znajek (1977). Their results can be analyzed as an electric circuit (Frank et al. 2002); hence, the black hole region should be included in our Central Column 0D model. The main uncertainty would be a loss of magnetic confinement in the jet, which then gives a back reaction on the disk that could upset the magnetically dominated equilibrium of our model. We return to this point in Paper II, with the conclusion that nonetheless, magnetic forces probably do dominate jet propagation.

6. DISCUSSION AND COMPARISON WITH OTHER MODELS

As stated in the introduction, one of our eventual goals is to find an explanation of UHECRs. While not all AGNs produce strong magnetic jets, it has long been recognized that those that do so could easily produce the 10^{20} V ($\sim 3 \times 10^{17}$ statvolts) needed to produce 10^{20} eV UHE cosmic rays (Lovelace 1976; Lynden-Bell 2006). Our numbers for the disk voltage, Equation (28), verify this if the disk viscosity ν is low enough. However, although ideas have been proposed (Colgate & Li 2004; Lyutikov & Ouyed 2007), there is no consensus on an accelerator mechanism to convert the dynamo voltage to 10^{20} eV UHECRs.

In this paper, we take the first step toward deriving a uniquely defined disk/jet accelerator. We do this by showing that the properties of the disk determine the correct boundary conditions that pin down the magnetic structure of the jet/accelerator, thereby selecting the actual solution out of all possible jet solutions as obtained via the Grad-Shafranov solutions.

A key feature of our model is the separation of the accretion disk into zones, the Central Column zone where most of the dynamo current enters the jet, and the Diffuse Pinch zone surrounding this Central Column in which disk rotation is nearly Keplerian. Though producing only a fraction of the power, it is the Diffuse Pinch zone that accounts for the remarkable stability of jets and eventual creation of the giant radio-lobes whose magnetic inductance will dictate jet propagation and ion acceleration.

Three features of our Diffuse Pinch model differ from previous models and simulations. First, the Diffuse Pinch zone of our jet is launched with $B_r = 0$, foretelling in subsequent papers a jet "tower" propagating with straight flux surfaces out to the Nose, as in Figure 1. To our knowledge, general relativistic MHD (GRMHD) codes modeling accretion disks from first principles do not yet exhibit sustained straight jets that are long when compared to disk dimensions. Yet, for a jet lengthening slowly compared to Alfvén velocities as predicted for our model, away from disk gravity a symmetrically averaged jet solution must satisfy the Grad-Shafranov equation that invariably produces jets that straighten within a large distance compared to the dynamo radius, however they are launched. Only non-magnetic pressure inside the Central Column exceeding the magnetic pressure could destroy the collimation giving straight jets. We will return to this point in subsequent papers.

Second, we find that the condition for a strong jet gives $B_r/B_\phi \ll 1$ even inside the disk, by Equation (9) and Appendix A. This precludes a significant role for centrifugal ejection of jet plasma in the Diffuse Pinch, as proposed by Blandford & Payne (1982) and explored extensively in the

literature, both concerning the effect of centrifugally ejected winds on jet propagation and the mechanisms whereby tilting of field lines develops inside the disk. The effects of winds on jets are explored in Grad-Shafranov solutions applying fluid constants of the motion as constraints characterized by a Mach number v/v_A (Alfvén velocity), recently reviewed by Beskin (Beskin 2010 and references therein: e.g., Heyvaerts & Norman 1989; Appl & Camenzind 1993; Beskin & Nokhrina 2009). By contrast, we will show in Paper II that the absence of line tilt derived from the hyper-resistive Ohm's Law in Equation (10) leads to the electrostatic ejection of the jet giving a low jet density and an Alfvén velocity greatly exceeding the velocity of jet evolution, and hence negligible Mach numbers. Concerning field line tilt inside the jet, the difference between our result with negligible field tilt and numerous papers in the literature can again be traced to our usage of the hyper-resistive Ohm's Law versus formulations characterized by a resistive Prandtl number (e.g., Ferreira & Pelletier 1993, 1995; Ferreira 2003; Ogilvie & Livio 2001; Ogilvie 2012; Guilet & Ogilvie 2012, 2013; Bisnovatyi-Kogan & Lovelace 2007; Rothstein & Lovelace 2008; Lovelace et al. 2009; Bisnovatyi-Kogan & Lovelace 2012).

Third, compared to other quasi-static models of jets (e.g., Li et al. 2001; Lynden-Bell 2003), we find that the proper boundary condition is the coronal field of our model, rather than the "winding" condition in those papers. This is the result of radial diffusion of the current inside the disk. Again, we will return to this point in subsequent papers.

Finally, unlike accelerators in the tradition of the transient Fermi model, in subsequent papers, we will show that the disk voltage in Equation (28) is continuously available to provide steady-state acceleration of ions and electrons in the jet (see also Colgate & Li 2004). The formulas in Section 5.2 and the accretion disk magnetic profile in Figure 2 and Equation (18) provide all of the information needed to calculate jet formation and propagation with electron and UHECR acceleration in subsequent papers.

T.K.F., H.L., and J.P. report with sadness that our coauthor Stirling Colgate, who instigated this work and contributed seminal ideas, passed away 2013 December 1. We thank the referees for their comments that improved the clarity of the paper. T.K.F. acknowledges many useful conversations with Roger Blandford and Jonathan McKinney. We thank R. H. Bulmer for the use of Figure 1 adapted from Fowler et al. (2011). We gratefully acknowledge the support of the U.S. Department of Energy Office of Science through the Center for Magnetic Self-Organization and through the LANL/LDRD Program for this work. J.P. acknowledges support at LLNL under U.S. Department of Energy contract DE-AC52-07NA27344.

APPENDIX A

HYPER-RESISTIVE OHM'S LAW, CLOSURE OF THE MODEL, AND ESTIMATE OF G

In Section 4 of the main text, we identified an ordering scheme with $|v_r/v_K| \ll 1$ necessary to obtain the strong magnetic jets associated with radio-loud AGNs. This Appendix completes the heuristic argument to justify Equation (9) and the ordering scheme.

A.1. Hyper-resistivity Ordering

We obtain the hyper-resistivity $\mathcal{D} = -c^{-1}\langle \mathbf{v}_1 \times \mathbf{B}_1 \rangle$ by estimating fluctuations $\mathbf{v}_1$ and $\mathbf{B}_1$ from linearized equations as in quasi-linear theory (Krall & Trivelpiece 1973). Otherwise, we maintain generality, first by taking $\langle ... \rangle$ as the same symmetric average over fluctuations in time and space used to derive Equations (4) and (5) so that $\mathbf{v}_1$ and $\mathbf{B}_1$ can represent any kind of fluctuations including symmetric MRI modes; and second, by deriving $\mathbf{v}_1$ from the linearized Ohm's Law applicable for any cause of fluctuations in the momentum equation, including external disturbances (Pariev & Colgate 2007). We write the following:

$$\mathbf{E}_1 = -c^{-1}\partial \mathbf{A}_1/\partial t - \nabla \Phi_1 = -c^{-1}(\mathbf{v}_1 \times \mathbf{B} + v_\phi \hat{\phi} \times \mathbf{B}_1). \quad \text{(A1)}$$

Here the smooth-averaged $v_\phi \hat{\phi}$ represents disk rotation, and we ignore accretion $v_r \ll v_\phi$. We take $\mathbf{v}_1$ and $\mathbf{B}_1$ to be real numbers (no Fourier transform). In evaluating $\mathcal{D}$ in Equation (10), we will assume that $\langle ... \rangle$ is restricted to perturbations favorably correlated to produce the sustained transport. Only 3D simulations can determine the validity of this assumption.

Equation (A1) only determines $\mathbf{v}_{1\perp}$ perpendicular to $\mathbf{B}$ and only $\mathbf{v}_{1\perp}$ affects $\mathbf{B}_1$ through the linearized Faraday's Law $\partial \mathbf{B}_1/\partial t = \nabla \times (\mathbf{v}_1 \times \mathbf{B} + \mathbf{v} \times \mathbf{B}_1)$. We will limit our discussion to the impact of $\mathbf{v}_{1\perp}$ on $\mathcal{D}$ whereby $\mathbf{v}_{1\perp}$ can be evaluated by operating by $(\times \mathbf{B})$ from the right on Equation (A1), giving

$$v_{1r} = B^{-2}(cE_{1\phi}B_z - cE_{1z}B_\phi + v_\phi B_{1r}B_\phi), \quad \text{(A2a)}$$

$$v_{1\phi} = B^{-2}(-cE_{1r}B_z - v_\phi B_{1z}B_z), \quad \text{(A2b)}$$

$$v_{1z} = B^{-2}(cE_{1r}B_\phi + v_\phi B_{1z}B_\phi). \quad \text{(A2c)}$$

Substituting Equations (A2a)–(A2c) into the RHS of Equation (10) gives

$$\begin{aligned} -c\mathcal{D}_\phi &= \langle v_{1z}B_{1r} - v_{1r}B_{1z} \rangle \\ &= B^{-2}\langle cE_{1r}B_\phi B_{1r} - \{cE_{1\phi}B_zB_{1z}\} + cE_{1z}B_\phi B_{1z} \rangle, \end{aligned} \quad \text{(A3a)}$$

$$\begin{aligned} -c\mathcal{D}_r &= \langle v_{1\phi}B_{1z} - v_{1z}B_{1\phi} \rangle \\ &= B^{-2}\langle \{(-cE_{1r}B_z - v_\phi B_{1z}B_z)B_{1z}\} \\ &\quad - (cE_{1r}B_\phi + v_\phi B_{1z}B_\phi)B_{1\phi} \rangle, \end{aligned} \quad \text{(A3b)}$$

$$\begin{aligned} -c\mathcal{D}_z &= \langle v_{1r}B_{1\phi} - v_{1\phi}B_{1r} \rangle \\ &= B^{-2}\langle (\{cE_{1\phi}B_z\} - cE_{1z}B_\phi + v_\phi B_{1r}B_\phi)B_{1\phi} \\ &\quad + \{(cE_{1r} + v_\phi B_{1z})B_zB_{1r}\} \rangle, \end{aligned} \quad \text{(A3c)}$$

where the cancellation of v_ϕ terms in Equation (A3a) is exact.

We now make further approximations to justify dropping all terms in $\{...\}$ in Equations (A3a)–(A3c). First, we apply the boundary conditions in Section 4 to give $v_{1z} = (H/r)v_{1r}$ for perturbations by analogy with Equation (12) for mean fields. Substituting v_{1z} and v_{1r} from Equations (A2a) and (A2c) into $v_{1z} = (H/r)v_{1r}$ gives $B_{1z} = (H/r)B_{1r}$ if we equate only the v_ϕ terms to give a result valid for any v_ϕ. Equating the remaining terms gives $E_{1z} = (r/H)E_{1r}$, if we drop $cE_{1\phi}B_z$, as we will approximate below that $E_{1\phi}$ is of the same order as E_{1r} but $B_z \ll B_\phi$.

Next, we approximate the field $\mathbf{B}$ inside the disk by the coronal field, even though B_ϕ falls to zero at $z = 0$. Then, using Equation (18), we take $B^2 \approx B_\phi^2$ and $B_z/B_\phi \approx (H/z)(a/r)^{1/2} \ll 1$ valid over much of the disk. Finally, we

also assume $B_{1\phi} \approx B_{1r}$ and $E_{1\phi} \approx E_{1r}$, giving altogether the following set of simplifications inside the disk:

$$B^2 \approx B_\phi^2;\ B_z/B_\phi \ll 1;\ B_r \approx 0, \tag{A4a}$$

$$B_{1r} \approx (r/H)B_{1z} \approx B_{1\phi}, \tag{A4b}$$

$$E_{1r} \approx (H/r)E_{1z} \approx E_{1\phi}. \tag{A4c}$$

At the end of this Appendix, we discuss why it is our focus on transport leading to accretion that leads to these assumptions. Given Equations (A4a)–(A4c), we can drop all terms in {...} in Equations (A3a)–(A3c) to obtain $\mathcal{D}$ and from this our ordering scheme using Equation (14). We first give results and then discuss how they are obtained. We have

$$-c\mathcal{D}_\phi = \langle cE_{1r}B_{1r}/B_\phi + cE_{1z}B_{1z}/B_\phi\rangle \approx \langle cE_{1r}B_{1r}/B_\phi\rangle, \tag{A5a}$$

$$\begin{aligned} -c\mathcal{D}_r &= -\langle cE_{1r}B_{1r}/B_\phi + (v_\phi/B_\phi)(B_{1z}B_{1\phi})\rangle \\ &\approx c\mathcal{D}_\phi(1+\zeta X), \end{aligned} \tag{A5b}$$

$$-c\mathcal{D}_z = \langle -cE_{1z}B_{1\phi}/B_\phi + (v_\phi/B_\phi)B_{1r}B_{1\phi}\rangle \approx (r/H)c\mathcal{D}_r, \tag{A5c}$$

where again $\zeta = HB_\phi/(rB_z)$ and X is given by

$$\begin{aligned} X &= \langle (v_\phi B_{1r}/B_\phi)^2/v_r v_\phi\rangle \lesssim \left\langle v_{1r}^2/v_r v_\phi\right\rangle \approx \gamma/\Omega \\ &\approx (|v_r/v_\phi|/\zeta)^{1/2} \approx |v_r/v_\phi|^{1/2}. \end{aligned} \tag{A6}$$

Substituting Equations (A5a)–(A5c) into Equation (14) gives

$$\begin{aligned} \zeta &\equiv (HB_\phi/rB_z) \approx \mathcal{D}_r/\mathcal{D}_\phi \\ &\approx 1+\zeta X < 1+(\zeta|v_r/v_\phi|)^{1/2} \approx 1, \end{aligned} \tag{A7}$$

$$\begin{aligned} |B_r/B_\phi| &\approx |(v_r/v_\phi) - (c\mathcal{D}_z/v_\phi B_\phi)| \\ &\approx |(v_r/v_\phi)|(1+\zeta^{-1}+X) \approx |v_r/v_\phi|, \end{aligned} \tag{A8}$$

and finally our ordering parameter justifying Equation (9) in the main text:

$$\delta r/r = (HB_r/rB_z) = \zeta|B_r/B_\phi| \approx |v_r/v_K|. \tag{A9}$$

Results on the far RHS of Equations (A6)–(A9) are obtained by expansions to the lowest order in our ordering parameter $\epsilon = |v_r/v_K|^{1/2}$, and equating $v_\phi = r\Omega \approx v_K = r\Omega_K$ anticipates $\Omega \approx \Omega_K$ in Appendix A.2.

In Equation (A5a), we have used $E_{1z} \approx (r/H)E_{1r}$ from Equation (A4c) which shows that the two terms are of the same magnitude; so, signs being uncertain, we approximate the sum of terms by one such term. In Equation (A5b), the term with ζX comes from $(v_\phi/B_\phi)(B_{1z}B_{1\phi})/(c\mathcal{D}_\phi)$ with $B_{1\phi} = B_{1r}$ and $B_{1z} = (H/r)B_{1r}$ from Equation (A4b) and $c\mathcal{D}_\phi = -v_r B_z$ from Equation (13); Equation (A5c) is obtained similarly.

To obtain Equation (A6), first we have used $v_\phi(B_{1r}/B_\phi) < v_{1r}$ from Equation (A2a). Then, using transport theory, we take a transport step to be $\delta x = (v_{1r}/\gamma)$ for a correlation time $1/\gamma$ at non-linear saturation, and from this a diffusion coefficient $D_a = \gamma(\delta x)^2$ giving $v_r = D_a/r$, hence $v_{1r}^2 = r\gamma v_r$, from which $\langle v_{1r}^2/v_r v_\phi\rangle \approx \gamma/\Omega$.

The final step in Equation (A6) is suggested by the following. For fluctuations such as MRI that are driven by disk rotational shear, the saturated value of γ is probably determined not by a relaxation of rotational shear but rather by self-adjustment of the z wave number k to the disk height H. This suggests that the system hovers near the threshold for MRI, which we approximate as $kv_{Az} \approx \gamma$ for $v_{Az}^2 = (B_z^2/4\pi\rho)$. Using Equations (3) and (7) to evaluate ρ, this condition yields $\gamma/\Omega \approx (k^2H^2/2)[|v_r/v_\phi|/\zeta]^{1/2} \approx (|v_r/v_\phi|/\zeta)^{1/2}$.

To summarize, given Equation (A6), we can derive Equations (A7)–(A9) in the limit that $|v_r/v_\phi| \ll 1$. This set of equations confirms the ordering relationships used in the main text.

In addition, we emphasize that the hyper-resistivity $\mathcal{D}$ treatment here represents a major difference between our work and the previous studies of Ferreira, Lovelace, and Ogilvie, among others, as cited in Section 6, which have employed $\mathcal{D} = \eta\mathbf{j}$ with an isotropic scalar resistivity η. This difference can be illustrated as follows: both Lovelace et al. (2009) and Guilet & Ogilvie (2012) take $\mathcal{D}_\phi = \eta j_\phi \propto \eta(-B_z/r + B_r/H) \approx \eta B_r/H$ for a thin disk. Contrary to Equation (A8), if η were small, substituting $\mathcal{D}_\phi \approx \eta B_r/H$ into Equation (13) could lead to a large $B_r \approx B_z(H/r)(4\pi r v_r/\eta c^2)$.

That the approximations leading to our $\mathcal{D}$ follow from our focus on accretion transport is suggested by the following. First, we replace Equation (A4b) by

$$A_{1r} \approx (H/r)A_{1z} \approx A_{1\phi}. \tag{A10}$$

In evaluating $\mathbf{B}_1 = \nabla\times\mathbf{A}_1$, the focus on transport suggests that we approximate $\partial/\partial r \approx 1/r \approx k_r$; $\partial/\partial z \approx 1/H \approx k_z$; and $r^{-1}(\partial/\partial\phi) \approx m/r \approx 1/r \approx k_\phi$ giving the largest transport because the transport coefficient is typically $\approx\gamma/k^2$, where hereafter $\gamma < \Omega$ is the reciprocal correlation time at nonlinear saturation (Kadomtsev 1965). Then applying Equation (A10) to $\nabla\times\mathbf{A}_1 = \mathbf{B}_1$ gives Equation (A4b), so Equations (A10) and (A4b) are equivalent. Moreover, for the above wave numbers, one can show that $\partial\mathbf{B}_1/\partial t = -\nabla\times(c\mathbf{E}_1)$ yields $B_{1\phi} \approx B_{1r}$ using $B_{1z} \approx (H/r)B_{1r}$ that was shown to follow from $v_{1z} \approx (H/r)v_{1r}$ in analogy with Equation (12), so to this extent Equations (A10) and (A4b) follow from theory. Finally, $\nabla\cdot\mathbf{E}_1 \neq 0$ for $\mathbf{E}_1$ in Equation (10), with $\mathbf{v}_1$ from Equations (A2a)–(A2c) indicating the existence of an electrostatic charge perturbation. In fact, $\mathbf{E}_1 = -\nabla\Phi_1 \gg -c^{-1}\partial\mathbf{A}_1/\partial t$ using Equation (A10) with $\partial/\partial t \approx \omega$, giving $(\partial A_{1r}/\partial t)/(c\Phi_1/r) \approx (\omega/\Omega)\zeta X$, which is $\ll 1$ with $\omega < \Omega$ for rotation-driven fluctuations; and similarly for $A_{1\phi}$ and A_{1z}. Hence, we can take $\mathbf{E}_1 \approx -\nabla\Phi_1$ giving Equation (A4c), of importance also in simplifying the discussion of Appendix B.

A.2. Estimate of the Viscosity Factor g and Disk Properties

As noted in Section 4.2, the main physics determining whether magnetic jets are strong or weak is contained in the quantity g defined by Equation (8). One issue is the viscosity ν, which must be small to obtain $g \approx 1$ giving a strong jet. The other is the rotation frequency $\Omega = \Omega_K - \delta\Omega$. In this appendix, we evaluate ν and $\delta\Omega$ in terms of our smallness parameter $|v_r/v_K|$ which we leave undetermined, as it depends on the unknown saturation level of fluctuations. Anticipating that $\delta\Omega$

is small, we can expand g in Equation (8) to give

$$g = [(\dot{M}/2)\Omega_K]^{-1}\int_0^H dz(4\pi/r)\partial/\partial r \times \{r\rho|v_r|r^2\Omega[1+(\nu/|v_r|)\partial(\ln\Omega)/\partial r]\} = 1-\left(\frac{2}{\dot{M}\Omega_K}\right)\left(\frac{2}{r}\right)\frac{\partial}{\partial r}\left\{\int_0^H dz(2\pi r\rho|v_r|)r^2\Omega_K \times\left[\frac{3\nu}{2r|v_r|}+\frac{\delta\Omega}{\Omega_K}+\frac{\nu}{|v_r|}\frac{1}{\Omega_K}\frac{\partial\delta\Omega}{\partial r}\right]\right\} \approx 1, \quad \text{(A11)}$$

where the leading unity term follows using the facts that Ω_K is independent of z and $\dot{M}$ is independent of r by Equation (3).

We first consider the viscous correction. The standard disk model assumes that viscosity $\nu \approx Hc_S = H^2\Omega$ whereby the standard model itself yields $3\nu/(2r|v_r|) \approx 1$ (Frank et al. 2002), which gives $g \approx 0$. The standard model also calculates the sound speed as $c_S = (\Gamma_{ad}p/\rho)^{1/2} \approx (T_e/m_i)^{1/2}$ (where Γ_{ad} is the adiabatic index) assuming a complete coupling of ion accretion energy to electron heat, which then determines H in the viscosity.

Here we take a different point of view that yields $\nu/(r|v_r|) \ll 1$, hence $g \approx 1$ as is required for accretion disks to produce strong magnetic jets. We take $\nu \propto \langle v_{1r}v_{1\phi} + v_{A1r}v_{A1\phi}\rangle$ (Balbus & Hawley 1998, Equation (35)), where the Alfvén velocities approximate the torque due to $\langle \mathbf{j}_1 \times \mathbf{B}_1\rangle$. For a strong dynamo dominated by the mean-field magnetic torque on the RHS of Equation (7), we find that the magnetic contribution is negligible compared to the mean field, of the order of $r(4\pi/c)\langle \mathbf{j}_1 \times \mathbf{B}_1\rangle_\phi/[\partial(rB_zB_\phi)/\partial z] \approx (B_{1r}/B_\phi)^2 < \epsilon^3$, where again we eliminate $\partial/\partial z \approx 1/H$ using Equation (A8) and using $(B_{1r}/B_\phi)^2 < (\gamma v_r/\Omega v_\phi) \approx \epsilon^3$ as in deriving Equation (A7).

Concerning velocity perturbations, we note that, for strong fluctuations, both the stress tensor giving ν and pressure giving departures from Keplerian rotation depend on ion velocity fluctuations, even though collisional coupling of ions and electrons is strong for accretion disk parameters. The reason is that, since in 3D MHD ions and electrons flow together, collisions only couple ion motion in the moving frame of the fluid while the coupling of ion velocity fluctuations to electron heat may be weak. Applied to viscosity, this says that the averaging over the product of particle velocities v_rv_ϕ giving the LHS of the mean field angular momentum equation, Equation (5), also contributes a randomly correlated fluctuation product $\langle v_{1r}v_{1\phi}\rangle$ which can dominate the stress tensor determining viscosity. Let $T_{r\phi} \approx \rho\langle v_{1r}v_{1\phi}\rangle \approx \rho\nu\Omega$ giving $\nu/(rv_r) = \langle v_{1r}^2/v_rv_\phi\rangle(v_{1\phi}/v_{1r}) \approx (\gamma/\Omega)(v_{1\phi}/v_{1r}) = |v_r/v_\phi|^{1/2}(a/r)$, where we have first used Equation (A6) and then Equations (A3a)–(A3c) giving $v_{1\phi}/v_{1r} \approx (H/r)(B_z/B_\phi) = \zeta(B_z/B_\phi)^2 \approx a/r$ by Equation (18) if we again extrapolate the coronal field inside the disk as in Appendix A.1. Thus, in contrast with the standard model that sets $\nu/(r|v_r|) \approx 1$ giving $g \approx 0$, our accretion-weighted viscous correction to g is very small at large r and order $\epsilon = |v_r/v_K|^{1/2} \approx |v_r/v_\phi|^{1/2}$ as $r \to a$, giving $g \approx 1$.

To determine $\delta\Omega/\Omega_K$, we return to Equation (4), already applied in the corona in deriving Equation (6). Here we apply Equation (4) inside the disk. We take terms in {...} to be zero compared to the RHS, justified below. Dividing by the gravitational force $\rho r\Omega_K^2$, we obtain

$$(\Omega/\Omega_K)^2[1+(1/4)(v_r/v_K)(a/r)] + (1/\Gamma_{ad})(c_S/v_K)^2 = 1. \quad \text{(A12)}$$

Here we neglect the B_ϕ term deep inside the disk, while $B_z^2/8\pi$ gives the term $\propto |v_r/v_K|$ in [...] using Equations (3) and (7) to express density as $\rho = (rB_\phi B_z)/(g\Omega_K 2\pi r v_r H)$ and using Equation (A7) to eliminate H. Scalings for B_z and B_ϕ according to Equation (18) are used as well. Pressure contributes the sound speed $c_S \approx (\Gamma_{ad}p/\rho)^{1/2}$. Similarly, both the magnetic term and the advective terms in {...} are found to be of the order of $|v_r/v_K|^2$ compared to gravity, hence smaller than terms retained in Equation (A12), and $[(\nabla\cdot\mathbf{T})_r/\rho r\Omega_K^2] \approx (\rho v_{1z}v_{1r}/H\rho r\Omega_K^2) \approx |v_r/v_K|(\gamma/\Omega_K) \approx |v_r/v_K|^{3/2}$, all of which justify dropping terms inside {...}.

The sound speed can be calculated in terms of $|v_r/v_\phi|$ using the force balance parallel to $\mathbf{B}_{\rm POL}$ in order to include the centrifugal force $(\rho v_\phi^2/r)(B_r/B_z) = (\rho v_\phi^2/H)(\delta r/r)$ with $\delta r/r \equiv (HB_r/rB_z)$ as in Equation (9). Dropping terms in this near-vertical force balance argued to be small in Lovelace et al. (2009) and dividing by $(\rho v_\phi^2/H)$, we obtain the following after some algebra:

$$(g/4)(v_r/v_\phi) + [\delta r/r(1-(3/2)H^2/r^2) + (H/r)^2] \approx (1/\Gamma_{ad})(c_S/v_\phi)^2 + \delta r/r. \quad \text{(A13)}$$

The centrifugal force term is on the far RHS, together with the vertical pressure term. The first term on the LHS is the vertical magnetic force $B_\phi^2/(8\pi H)$ using Equations (3), (7), and (A7) to relate ρ to B_ϕ. The terms in [...] come from gravity, $\rho\nabla\Phi_G\cdot(\mathbf{B}_{\rm POL}/B_{\rm POL})$, with $\Phi_G = -GM/(r^2+z^2)^{1/2} = -v_\phi^2[r/(r^2+z^2)^{1/2}]$ and expanding $(r^2+z^2)^{-3/2} \approx 1-(3/2)z^2/r^2$. The field tilt condition in Blandford & Payne (1982) follows if we ignore the magnetic term on the far LHS of Equation (A13), giving centrifugal ejection if $\delta r/r > 2/3$ versus their exact $\delta r/r > \cot 60^\circ = 0.6$. For our small $\delta r/r$, we obtain

$$(c_S/v_\phi)^2 \approx (g/4)(v_r/v_\phi) + (H/r)^2. \quad \text{(A14)}$$

The growth of velocity fluctuations $\mathbf{v}_1$ discussed in Appendix A.1 contributes to c_S, but for weak saturation levels, further compression of these fluctuations by magnetic and gravitational forces is required to reach the steady-state balance of forces in Equation (A13).

Except near $r = a$, the disk is compressed vertically by the magnetic pinch force rather than gravity, occurring when $H/r \ll (v_r/v_\phi)^{1/2}$ in Equation (A14). Then introducing Equation (A14) into Equation (A12) gives Keplerian rotation to order $|v_r/v_\phi|$. At smaller r, gravity prevails giving $1/2(c_S/v_\phi)^2 \approx (H/r)^2$ with $H/r = B_z/B_\phi = (a/r)^{1/2}(\Omega/\Omega_K)$ by Equations (A7) and (18) using g in Equation (A11). Then both the outward pressure $\propto (a/r)\Omega^2$ and the smaller magnetic term $B_z^2/(8\pi\rho v_\phi^2) \propto |v_r/v_\phi|(a/r)\Omega^2$ add to the outward centrifugal force, giving a departure from Keplerian rotation near $r = a$, but only as $\Omega/\Omega_K \to [1+(a/r)]^{-1/2} \geqslant 0.7$.

Concerning optical radiation by electrons, the standard model takes $c_S \approx (T_e/m_i)^{1/2}$ which gives optical radiation consistent with observations (Krolik 1999; Frank et al. 2002), but the standard model c_S/v_ϕ is inconsistent with Equation (A14) using Equation (14) for H. If our larger c_S produces shock heating of electrons, one could obtain $c_S \gg (T_e/m_i)^{1/2}$, which is consistent with our model but also consistent with a significant heating of electrons giving the observed optical spectra as in the standard model.

APPENDIX B

ORIGIN OF DYNAMO MAGNETIC FIELDS AND HELICITY CONSERVATION

Creating a self-excited dynamo in which poloidal flux $\Psi = rA_\phi$ grows in situ requires defeating Cowling's anti-dynamo theorem for axisymmetric fields. Using Equation (10) as a more general form for Ohm's Law and focusing on the ϕ component, we get

$$\partial\Psi/\partial t + \mathbf{v}_{\rm POL}\cdot\nabla\Psi = -rc\mathcal{D}_\phi, \quad \text{(B1)}$$

whereby ideal MHD fluid motion gives $\mathcal{D}_\phi = 0$, showing that in the absence of 3D fluctuations, flux can be advected but it cannot be created (Moffatt 1978; Balbus & Hawley 1998). In addition, if $\mathcal{D}_\phi$ is approximated as resistance, $\mathcal{D}_\phi = \eta j_\phi$ only dissipates flux.

That an accretion-driven dynamo does create flux can be shown as follows. Using Equation (18), the flux is given by $\Psi(r) = \int_0^r r dr B_z(r) = a^2 B_a[1+2[(r/a)^{1/2}-1]]$, where $r \leqslant R_0$ and R_0 is the O-point radius. By Equation (25), $aB_a \propto M^{1/2}$ for fixed τ in $\dot{M} = M/\tau$ and $a \propto M$ by Equation (27). Then we find that $\Psi(r) \propto M$ at large r and $\Psi(r) \propto M^{3/2}$ at small r, so that $\Psi(r)$ grows as $M = \dot{M}\tau$ grows, at all r. This is true even though $|B_z| \approx (aB_a)/a \propto M^{-1/2}$, which actually decreases with time. It is, however, not so easy to prove using Equation (B1), which says that the poloidal flux growth can indeed occur if there exists a small imbalance in Equation (13) to give $c\mathcal{D}_\phi = -v_r B_z + |\Psi|/(r\tau)$ at all r (note that we have used our sign convention that B_z is negative for $r < R_0$).

How flux is created is perhaps best understood through the role of $\mathcal{D}_\phi$ in helicity transport. The global helicity, defined by $K = \int d\mathbf{x}\mathbf{A}\cdot\mathbf{B}$, describes twisted magnetic fields with vector potential $\mathbf{A}$ giving $\mathbf{B} = \nabla\times\mathbf{A}$. Global helicity is useful because the mean-field helicity is conserved, since random 3D disturbances create no net helicity (Taylor 1986; Boozer 1986a; Bhattacharjee & Hameiri 1986; Vishniac & Cho 2001; Fowler & Gatto 2007; Blackman 2012). Averaging over fluctuations, we obtain the equation for mean-field helicity conservation:

$$\begin{aligned}\partial\langle\mathbf{A}\cdot\mathbf{B}\rangle/\partial t + \langle 2c\mathcal{D}\cdot\mathbf{B}\rangle &= -\nabla\cdot\langle\mathbf{A}\times\partial\mathbf{A}/\partial t + 2c\Phi\mathbf{B}\rangle \\ &\equiv -\nabla\cdot\mathbf{\Gamma}, \quad \text{(B2)}\end{aligned}$$

where $\mathbf{\Gamma}$ is the mean-field helicity flux and we use Ohm's Law in Equation (10) to write $(\partial\mathbf{A}/\partial t)\cdot\mathbf{B} = -c(\mathbf{E}+\nabla\Phi)\cdot\mathbf{B} = -c(\mathcal{D}\cdot\mathbf{B} + \nabla\cdot(\Phi\mathbf{B}))$, where Φ being conveniently chosen in Coulomb gauge to represent charging of the disk.

Integrated over a volume of interest, the RHS of Equation (B2) yields surface terms accounting for the creation of tokamak plasmas in the laboratory by externally produced induction, via the term $\mathbf{A}\cdot\partial\mathbf{A}/\partial t$, and spheromak plasmas created by external electrostatic guns, through the term $\Phi\mathbf{B}$ (Boozer 1986b). Applied to the volume enveloping an accretion disk and all jets it creates, the surface is presumably devoid of helicity sources so that this expression shows that helicity cannot be created by the accretion disk. However, a jet ejected out of the disk certainly contains twisted fields and helicity. The explanation is that jets ejected up and down from the disk have helicity of opposite signs (Vishniac & Cho 2001), though local differences in dissipation may eliminate or alter one of the jets. For a dipole poloidal field, the equal and opposite ejection of helicity follows from the fact that the poloidal flux passing through the disk has the same sign above and below the disk, while the ejected current creating B_ϕ has opposite signs. For a quadrupole field, the poloidal flux reverses sign while the corresponding reversal in sign of the radial electric field in the disk interior gives poloidal current of the same sign above and below the disk. Thus, helicity conservation poses no difficulty in accounting for magnetic jets created by a magnetized, rotating accretion disk, which behaves like a spheromak with the electrostatic gun embedded inside.

It is the role of $\mathcal{D}_\phi$ in the conserved flow of helicity from its point of creation to the O point in the disk that accounts for the self-amplification of B_z flux, both in laboratory spheromaks and in accretion disk dynamos. Initially, the dynamo O point may be that of a weak seed field consisting patches of flux advected toward the black hole, each patch of mean field flux circulating around an O point at $r = R_0$ where the poloidal field is zero. The presence of a 2D poloidal flux component causes the rotating disk to charge up, positive or negative depending on the direction of the flux. The flux patch nearest to the black hole would receive the most gravitational power, allowing it to push away advected flux outside so that this nearest region of growing poloidal flux becomes the magnetized accretion disk of interest.

To highlight helicity flow by $\mathcal{D}_\phi$, we approximate Equation (B2) as follows. To estimate the magnitude of $\nabla\cdot\mathbf{\Gamma} \approx r^{-1}\partial(r\Gamma_r)/\partial r$ at the O point, we drop the mean field $\partial\mathbf{A}/\partial t \approx A/\tau$ and we drop $\mathbf{A}_1\times\partial\mathbf{A}_1/\partial t$ (order ζX) giving as dominant terms:

$$2c\mathcal{D}_\phi B_\phi \approx -r^{-1}\partial(r\Gamma_r)/\partial r \approx -r^{-1}\partial\langle 2cr\Phi_1 B_{1r}\rangle/\partial r. \quad \text{(B3)}$$

A successful dynamo will require that the helicity flux from the fluctuations is such that $\mathcal{D}_\phi$ is positive at the O point. Then, according to Equation (B1), one expects that the O-point radius will grow to accommodate the poloidal flux growth. We will return to this important issue in a more quantitative estimate in subsequent papers by deriving R_0, which we will eventually identify as the outer limit of the jet radius.

REFERENCES

Appl, S., & Camenzind, M. 1993, A&A, 274, 699
Balbus, S. A., & Hawley, J. F. 1998, RvMP, 70, 1
Beckwith, K., Hawley, J. F., & Krolik, J. H. 2008, ApJ, 678, 1180
Beskin, V. S. 2010, PhyU, 53, 1199
Beskin, V. S., & Nokhrina, E. E. 2009, MNRAS, 397, 1486
Bhattacharjee, A., & Hameiri, E. 1986, PhRvL, 57, 206
Bisnovatyi-Kogan, G. S., & Lovelace, R. V. E. 2007, ApJL, 667, L167
Bisnovatyi-Kogan, G. S., & Lovelace, R. V. E. 2012, ApJ, 750, 109
Blackman, E. G. 2012, PhyS, 86, 058202
Blandford, R. D. 1976, MNRAS, 176, 465
Blandford, R. D., & Payne, D. G. 1982, MNRAS, 199, 883
Blandford, R. D., & Znajek, R. L. 1977, MNRAS, 179, 433
Boozer, A. H. 1986a, JPlPh, 35, 133
Boozer, A. H. 1986b, PhFl, 29, 4123
Bridle, A. H., & Perley, R. A. 1984, ARA&A, 22, 319
Burbidge, G. R. 1956, ApJ, 124, 416
Colgate, S. A., & Li, H. 2004, CRPhy, 5, 431
Colgate, S. A., Beckley, H., Si, J., et al. 2011, PhRvL, 106, 175003
Ebrahimi, F., & Prager, S. C. 2011, ApJ, 743, 192
Ferreira, J. 2003, arXir:astro-ph/0311621v1
Ferreira, J., & Pelletier, G. 1993, A&A, 276, 637
Ferreira, J., & Pelletier, G. 1995, A&A, 295, 807
Fowler, T. K. 2004, Lawrence Livermore National Laboratory Report, UCRL-TR-204727
Fowler, T. K., Colgate, S. A., Li, H., Bulmer, R. H., & Pino, J. 2011, Lawrence Livermore National Laboratory Report, LLNL-TR-474338
Fowler, T. K., & Gatto, R. 2007, PPCF, 49, 1673
Frank, J., King, A., & Raine, D. 2002, Accretion Power in Astrophysics (3rd ed.; Cambridge: Cambridge Univ. Press)
Guilet, J., & Ogilvie, G. I. 2012, MNRAS, 424, 2091
Guilet, J., & Ogilvie, G. I. 2013, MNRAS, 430, 822

Heyvaerts, J., & Norman, C. 1989, ApJ, 347, 1055
Hooper, E. B. 2012, PPCF, 54, 113001
Kadomtsev, B. B. 1965, Plasma Turbulence (New York: Academic Press)
Krall, N. A., & Trivelpiece, A. W. 1973, Principles of Plasma Physics (New York: McGraw-Hill)
Krolik, J. H. 1999, Active Galactic Nuclei (Princeton, NJ: Princeton Univ. Press)
Kronberg, P. P., Dufton, Q. W., Li, H., & Colgate, S. A. 2001, ApJ, 560, 178
Li, H., Lapenta, G., Finn, J. M., Li, S., & Colgate, S. A. 2006, ApJ, 643, 92
Li, H., Lovelace, R. V. E., Finn, J. M., & Colgate, S. A. 2001, ApJ, 561, 915
Lovelace, R. V. E. 1976, Natur, 262, 649
Lovelace, R. V. E., Rothstein, D. M., & Bisnovatyi-Kogan, G. S. 2009, ApJ, 701, 885
Lynden-Bell, D. 2003, MNRAS, 341, 1360
Lynden-Bell, D. 2006, MNRAS, 369, 1167
Lyutikov, M., & Ouyed, R. 2007, APh, 27, 473
Moffatt, H. K. 1978, Magnetic Field Generation in Electrically Conducting Fluids (Cambridge: Cambridge Univ. Press)
Ogilvie, G. I. 2012, MNRAS, 423, 132
Ogilvie, G. I., & Livio, M. 2001, ApJ, 553, 158
Pariev, V. I., & Colgate, S. A. 2007, ApJ, 658, 114
Rothstein, D. M., & Lovelace, R. V. E. 2008, ApJ, 677, 1221
Shakura, N. I., & Sunyaev, R. A. 1973, A&A, 24, 237
Solov'ev, L. S. 1963, in Voprosy Teorii Plazmy (Reviews of Plasma Physics), Vol. 3, ed. M. A. Leontovich (Moscow: Gosatomizdat), 245 [English translation (New York Consultants Bureau, 1967), 277]
Spruit, H. C. 2010, The Jet Paradigm (Lecture Notes in Physics, Vol. 794; Berlin: Springer), 233
Spruit, H. C., Stehle, R., & Papaloizou, J. C. B. 1995, MNRAS, 275, 1223
Taylor, J. B. 1986, RvMP, 58, 741
Vishniac, E. T., & Cho, J. 2001, ApJ, 550, 752